Composites: Part A 193 (2025) 108815

Contents lists available at ScienceDirect

Composites Part A

journal homepage: www.elsevier.com/locate/compositesa

Analytical prediction of the thermal overheating in curing thick layers of fibre-reinforced thermosets

Jordi Farjas [a,b,*], Daniel Sanchez-Rodriguez [a,b], Sihem Zaidi [b], Didina-Ramona-Casandra Cârstea [c,a], Ahmed Mohamed Saleh Abd Elfatah [b], Andrei Rotaru [d,e], Josep Costa [b]

[a] GRMT, Materials Research Group and Thermodynamics, Polytechnic School, University of Girona, Campus Montilivi, Edif. PII, E17003 Girona, Catalonia, Spain
[b] AMADE, Analysis and Advanced Materials for Structural Design, Polytechnic School, University of Girona, Campus Montilivi, Edif. PII, E17003 Girona, Catalonia, Spain
[c] Doctoral School of Sciences, Study Program for Chemistry, University of Craiova, Str. A.I. Cuza, Nr. 13, 200585 Craiova, Romania
[d] Department of Engineering Science, Babeş-Bolyai University, Str. Mihail Kogălniceanu, Nr. 1, 400084 Cluj-Napoca, Romania
[e] Department of Chemical Thermodynamics, Institute of Physical Chemistry–Ilie Murgulescu, Romanian Academy, Splaiul Independenţei, Nr. 202, 060021 Bucharest, Romania

ARTICLE INFO

Keywords:
Analytical model
Fibre-reinforced polymers
Composite materials manufacturing
Overheating
Overshooting
Thick laminates

ABSTRACT

A recurring problem when curing thick specimen carbon-fibre-reinforced polymers is the formation of thermal gradients. Thermal gradients can lead to heterogeneous properties, overcuring and, in some cases, matrix degradation. To address this problem, we have developed a general-purpose analytical solution that allows one to predict the maximum temperature difference within a specimen when the curing reaction takes place under isothermal conditions. The analytical solution is specifically tailored to deal with standard conditions in the manufacture of composites and can be applied to different resins and prepregs. In addition, it allows one to determine the conditions for when a thermal runaway will occur. The analytical solution was validated by comparing the analytical predictions with numerical and experimental results.

1. Introduction

Thick fibre-reinforced polymer (FRP) laminates are of practical interest for manufacturing pressure vessels for hydrogen storage [1], pressure pipes, for the aerospace industry [2–4], or to strengthen structural elements [5]. However, the combination of a high exothermal curing reaction together with the low thermal conductivity of epoxy resins can lead to thermal gradients forming within a specimen. In this context, manufacturers' recommended curing cycles (MRCC) commonly used for thin FRP panels may not be valid for thick laminates, thus resulting in undesirable effects such as overheating or even an overshoot. In addition, long curing cycles increase manufacturing costs and, consequently, in some applications high cure temperatures are used to promote fast curing and thus increase productivity [6]. Nonetheless, accelerating the cure cycle increases the rate of heat release during the cure cycle and can lead to the formation of thermal gradients, even in thin sections. Local overheating caused by a non-homogeneous curing process is detrimental to the mechanical properties. Besides, this can lead to residual stresses, surface waviness, matrix degradation and delamination, even for short-time processing [7–11]. In addition, when overheating exceeds a critical value, the heat generated locally by the curing process exceeds its dissipation, thus leading to a heat build-up that then further accelerates the curing process. As a result, the curing reaction becomes uncontrolled, with the local temperature increasing by tens or even hundreds of degrees. In this situation, the local temperature may exceed the degradation temperature, leading to a diminution of the mechanical properties or rejection of the component [7,12]. As such, developing a realistic analytical model to predict the degree of overheating as a function of the processing parameters is paramount, especially when working with thick parts or rapid curing cycles.

The common approach employed to deal with local overheating relies on numerical simulations [7,9,10,13–18] that consider heat

* Corresponding author at: GRMT, Materials Research Group and Thermodynamics, Polytechnic School, University of Girona, Campus Montilivi, Edif. PII, E17003 Girona, Catalonia, Spain.
E-mail address: jordi.farjas@udg.edu (J. Farjas).

https://doi.org/10.1016/j.compositesa.2025.108815
Received 10 January 2025; Received in revised form 14 February 2025; Accepted 18 February 2025
Available online 26 February 2025

diffusion through the specimen, heat transport at the boundaries, and heat generation. Bogetti and Gillespe [10] developed a 2D numerical simulation that revealed that thermal gradients may appear in thick-sections resulting in a non-uniform curing process. Twardowski *et al.* [9] using a 1D simulation reproduced the thermal gradients observed in a 5-cm-thick sample. In addition, they showed that it is reasonable to assume that the thermal properties of the resin and of the fibre during the curing process can be considered independent of the temperature and extent of reaction. Using numerical simulations and experimental data, Ruiz and Trochu [17] showed that curing at high temperature results in the build-up of temperature gradients that lead to critical internal stresses. Using a 3D simulation, Oh *et al.* [13] successfully reproduced the thermal gradients observed experimentally. They also showed that the thickness of the mould had little influence on the thermal behaviour of the system. Furthermore, they created a numerical optimization of the cure cycle to reduce temperature overshoot. Dolkun *et al.* [15] developed a cure cycle numerical optimization for thick parts based on a finite element analysis, while Leistner *et al.* [19] also generated a numerical simulation based on finite elements that considered the dependence on temperature and cure degree of the heat capacity and heat conductivity. Tifkitsis *et al.* [14] developed a multi-objective cure optimization methodology to minimize the overshoot using an autocatalytic kinetic model that also takes the effect of diffusion into account.

Although numerical simulations are accurate and provide reliable simulations, their implementation is complex, and computationally expensive to run. Conversely, analytical methods might be less precise but improve the knowledge about the process, thus allowing for an easier analysis of the effects of curing cycle parameters on the process, providing relevant information on the optimisation of the curing cycle, and facilitating decision-making concerning the design of the curing process of thick laminates or for fast curing laminates. Indeed, the analytical models simplify and accelerate the design of the curing cycles. To the best of our knowledge, to date only a single analytical criterion for the thermal runaway has been developed for polymer composites [20]. However this analytical model is limited to the prediction of the thermal runaway and does not consider convective losses.

In this work, we develop an analytical model that allows us to determine the critical thickness required to avoid the formation of a chosen temperature gradient for an isothermal curing cycle. The analytical solution is based on a heat diffusion model that takes convection heat losses into account. Besides, the model also provides the critical thickness required to prevent a thermal runaway. The model is validated against numerical simulations and experimental data from the curing process of a carbon-fibre-reinforced polymer (CFRP) with VTC401 epoxy component prepreg ("pre-impregnated" fibres with a partially cured polymer matrix).

2. Materials and methods

2.1. Composite's curing

The materials used in the experiments are CFRP laminates made of carbon epoxy prepreg VTC401 of 193 g/m^2 areal weight, carbon fibre sheet T700 and 42 % resin weight content from SHD Composite Materials Ltd (reference VTC401-C193-PW-T700-12 K-42 %RW-1270). We prepared seven 105 × 105 × w mm^3 panels, where w is 14.8, 21.5 or 26.5 mm − corresponding to 56, 82 and 110 layers, respectively. The prepreg sheets were deposited layer by layer. After depositing each layer, we use a roller to compress the panel and after each deposition of ten layers, we apply vacuum to ensure good compaction. The thicknesses given in Table 1 are the average values of four thicknesses measured at different positions. In all cases, the difference between the measured values and the average thickness is less than 0.3 mm.

The panels were fabricated with five embedded thermocouples (labelled 1 to 5 in Fig. 1) to measure the temperature evolution at different positions during the curing process. The thickness of the thermocouple is 1.2 mm. One thermocouple was placed on top of the first layer, another located below the last layer, and three more were equidistant within the laminate cross-section (see schematic in Fig. 1). Thermocouples are slightly offset from the centre of the cross-section to minimize panel distortion. To improve thermalisation during the curing experiments, the panels were placed on top of a 200 × 200 × 30 mm^3 steel plate. Two thermocouples were used to measure the temperature of the steel plate at two different positions (labelled 6 and 7 in Fig. 1).

Table 1
Maximum overheating measured in the laminate curing experiments together with the maximum overheat calculated by the numerical simulations.

Thickness mm	Cure temperature °C	Measured Overheating / °C	Calculated Overheating / °C
14.8	63	0.5	0.97
14.8	81	8	7.65
14.9	85	15	13.4
21.5	72	6	6.26
21.7	77	10	12.6
21.4	84	35	37.6
27.3	74	16	18.4
27.0	80	41	45.4
26.3	82	57	57.5

Curing experiments were performed by placing the laminate inside an oven that was kept at a constant target temperature. To minimize the drop in temperature when the laminate was placed in the furnace, the steel plate was also preheated inside the furnace to ensure that it was also at the target temperature when the laminate was introduced into the oven. With this configuration, the temperature drop in the steel plate when the laminate was introduced into the furnace was around 0.5 °C. Table 1 summarises the experiments carried out, as well as the maximum overheating recorded. The temperature evolutions recorded are shown in the supplementary information.

The thermal conductivity of the prepreg was measured with a homemade Poensgen apparatus (see supplementary information, Fig. S1). Two polymethyl methacrylate plates, one 4.10 mm and the other 3.75 mm thick, were used as reference material. A 2.60 mm thick uncured laminate was heated under a controlled heat flux until a stationary regime was reached. At steady state, the temperature at the bottom and top of the laminate was 40.3 and 37.7 °C, respectively. Given the planar geometry of the system, the heat losses through the thickness of the plate are negligible and the thermal conductivity was obtained from the one-dimensional expression of Fourier's law. Following this method, a thermal conductivity of $k = 0.23$ W/(m·K) was obtained.

The specific heat capacity, c, was measured using the method described in [21,22]. The heat capacity experiments were carried out using a Mettler Toledo DSC822e. For differential scanning calorimetry (DSC) measurements, a sample mass of 3.177 mg was placed inside a 40 µl aluminium crucible. During the measurements, a flow rate of 40 ml/min of high purity N_2 was established. A sapphire crystal of 26.06 mg was used as calibration material. The DSC curves of the sapphire and the laminate, and the heat capacities at temperatures of 50, 60 and 70 °C have been included in the supplementary information (Figs. S2 and S3, and Table S1).

The density was obtained by measuring the mass and volume of the manufactured laminates. We obtained very similar values for the nine manufactured panels; the standard deviation was 10 kg/m^3 and the density $\rho = 1210 \pm 7$ kg/m^3. This low standard deviation indicates that the panel production was reproducible.

The experiments were performed in a convective furnace; the air velocity inside the furnace was around 10 m/s. Under these conditions, the apparent convective coefficient h is around 40 W/(m^2·K) [23]. The thermal, kinetic and physical properties of the VTC401 prepreg are summarized in Table 2.

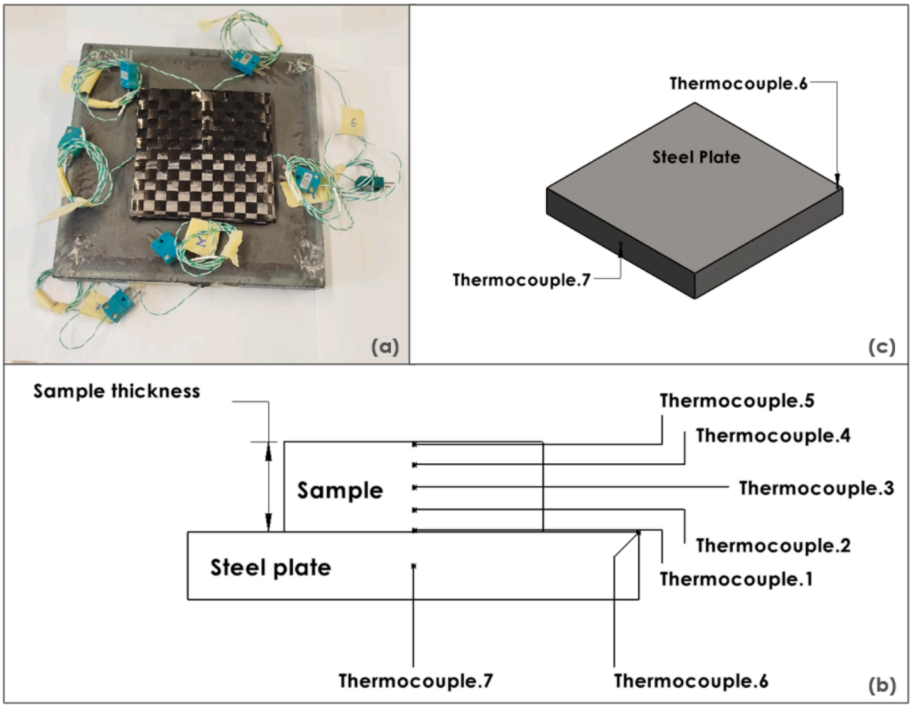

Fig. 1. (a) Manufactured 105 × 105 × 21.5 mm^3 CFRP panel with five embedded thermocouples. (b) Diagram of the cross-section of the laminate placed on a steel plate and (c) diagram of the positions of the two thermocouples placed on the steel plate.

Table 2
Measured physical parameters used in the numerical simulations and analytical calculations.

Property	Value
Thermal conductivity out-of-plane at 40 °C, k, W/(m·K)	0.23
Specific heat capacity at 60 °C, c, J/(kg K)	1250
Apparent convective coefficient, h, W/(m^2·K)	40
Density, ρ, kg/m^3	1210
Specific heat of reaction, q, J/kg	1.60×10^5
Activation energy, E_α, J/mol	8.84×10^4
Pre-exponential factor, A, 1/s	1.0×10^9

2.2. *Determining the specific heat of reaction and kinetic parameters*

To determine the specific heat of reaction and kinetic parameters, five DSC measurements were taken at heating rates, $\beta \equiv \frac{dT}{dt}$ of 0.6, 1.25, 2.5, 5 and 10 K/min. The time step for the data acquisition was 0.03 s. The DSC measurements were carried out on a TA Instruments Q2000 apparatus. Samples of mass around 2.3 mg were placed in sealed aluminium T-zero pans and the measurements were taken under a high purity nitrogen flow of 50 ml/min.

From the integration of the DSC signal we determined the specific heat of reaction; the average value was: $q = (1.60 \pm 0.05) \times 10^5$ J/kg. Likewise, under the assumption that the rate of reaction is proportional to the heat released, it was possible to determine the degree of curing from the DSC signal [24,25] – Eq. 1:

$$\frac{d\alpha}{dt} = \frac{1}{q}\frac{dq}{dt}, \tag{1}$$

where α is the degree of curing ($0 \leq \alpha \leq 1$) and dq/dt is the heat flow measured by the DSC. Fig. 2.a shows the evolutions of the degree of cure for the five experiments carried out at different heating rates.

Once the evolution of the degree of curing had been determined, the kinetics could be characterised using isoconversional kinetic methods. Isoconversional methods are commonly preferred over mode-fitting methods because no assumptions have to be made about the reaction model [26,27]. Furthermore, the isoconversional methods have been successfully used to characterize the curing kinetics of resins [28–37]. Based on the isoconversional approach [38], the kinetics can be described by the following relationship (Eq. 2):

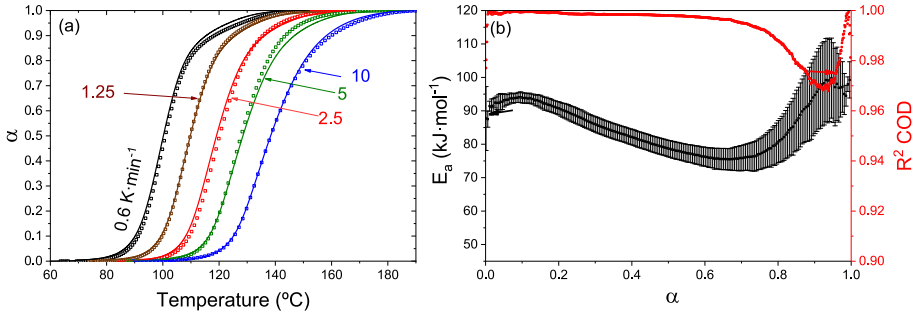

Fig. 2. (a) Curing degree evolution obtained from DSC experiments (squares) and predicted evolution according to Eq. 4 (solid lines). (b) Activation energy determined using Friedman isoconversional analysis and R^2 coefficient of determination of the Friedman linear fitting.

$$\left.\frac{d\alpha}{dt}\right|_{\alpha} = A_{\alpha}\exp\left[-\frac{E_{\alpha}}{R_G T_{\alpha}}\right] f(\alpha). \quad (2)$$

where T is the temperature, E_α is the activation energy at a certain conversion degree α, R_G is the gas constant, A_α is the preexponential term, and $f(\alpha)$ is the conversion function standing for the kinetic model of the reaction. Thus, the kinetics is fully described by the parameters E_α and $A_\alpha f(\alpha)$.

In particular, we have used Friedman's isoconversional method [39] which is the most straightforward method coming directly from the rate equation (Eq. 2). First, we discretised the degree of curing: $\alpha_j = j\Delta\alpha$, where j is a positive integer number, $0 \le j \le 1001$, and $\Delta\alpha = 0.001$. As we performed five experiments at different heating rates, β_i, from each experiment we were able to determine the temperature, $T_{j,i}$, and a transformation rate $\left.\frac{d\alpha}{dt}\right|_{j,i}$ corresponding to a cure degree α_j. Thus, according to Eq. 2:

$$\ln\left.\frac{d\alpha}{dt}\right|_{j,i} = -\frac{E_j}{RT_{j,i}} + \ln(Af(\alpha))|_j. \quad (3)$$

Therefore, there is a linear relationship between $\ln\left.\frac{d\alpha}{dt}\right|_{j,i}$ and the reciprocal of $T_{j,i}$. From the slope and the intercept of a linear fit we were able to determine the activation energy and $A_\alpha f(\alpha)$ related to a conversion degree α_j. In Fig. 2.b we have plotted the resulting activation energy together with the coefficient of determination R^2 of the linear fit.

The evolution of the activation energy shows that the curing process involves several stages: the high initial values of the activation energy may correspond to the uncatalyzed reaction, while the increase in the activation energy in the latter stages can be attributed to the diffusional delay caused by the increase in viscosity [40].

Once the kinetic parameters have been determined, we can then predict the evolution of the curing reaction for an arbitrary temperature program [41,42]:

$$\alpha_{k+1} = \alpha_k + Af(\alpha)|_k \bullet e^{-\frac{E_k}{RT}}\Delta t_k, \quad (4)$$

where $T_k = T(t_k)$ is the discretization of the temperature program, α_k, E_k and $Af(\alpha)|_k$ are α, E_α and $A_\alpha f(\alpha)$ for a given temperature T_k, and Δt_k is the time interval between T_k and T_{k+1}. To validate the kinetic analysis, we compared the predicted evolution with that obtained from the DSC measurement using the one measured by the DSC as thermal history; the T_k data set is obtained directly from the DSC recording. Fig. 2.a confirms that there is a good agreement between the measured and expected evolution of the curing reaction.

To verify that the isoconversional analysis is able to predict the reaction kinetics for an arbitrary temperature program, we have performed two different DSC experiments consisting of a constant temperature rise at 10 K/min up to a given temperature (130 °C or 150 °C) followed by an isothermal dwell time until a full degree of cure is achieved. The time required for full cure is determined from the isoconversional prediction. The results are shown in the supplementary information, see Figs. S4 and S5, and show a good agreement between the predicted and measured evolutions. In addition, we have also measured the glass transition temperature, T_g, to confirm that the samples are fully cured. For the experiments performed up to 130 °C and 150 °C we obtained a T_g of 133 °C and 128.5 °C respectively. According to the manufacturer, the maximum T_g of this prepreg is 130 °C, so we can confirm that in both cases the samples are fully cured. In Fig. S6 (supplementary information) we have plotted the DSC curves used to determine the T_g.

Note that the isoconversional analysis does not account for resin vitrification, so Eq. 4 will give inaccurate predictions for isothermal treatments below the maximum glass transition temperature. However, overheating occurs for cure rates around the maximum rate, typically for cure rates below 0.6. Therefore, to predict the overheating we need a reliable kinetic model for cure degrees below 0.6. To approach vitrification for a degree of cure of less than 0.6 we need to cure at a temperature far from those used in panel manufacturing. For example, for VTC401 we need to cure at temperatures below 50 °C and this means that the time we need to reach a degree of cure of 0.6 is more than 280 h. Therefore, to determine the overheating, it is reasonable to disregard vitrification.

2.3. The continuum model

In this section, we introduce a classical continuum model from which the approximate analytical model is derived in the next section. To check the accuracy of the analytical model, we compare it to the numerical integration of this continuum model. This model takes into account heat generation by the curing reaction and heat propagation. During curing, heat dissipation is more efficient in the outer parts of a panel than in its centre, so that the maximum local overheating is located in the centre of the panel [10,13,19,42]. For relatively flat panels, due to symmetry, in the central part of the panel, the thermal gradients in the laminate plane are negligible compared to the gradients along the direction perpendicular to the fibres (see temperature contours in [13]). Furthermore, Ren et al. [43] have shown that for high width to thickness ratio, in the central region the accuracy of the one-dimensional curing simulation can satisfy the engineering requirements. A validity criterion for the one-dimensional heat flow assumption is presented in the appendix. Thus, to determine the maximum overheating, the heat balance during the curing process can be described by a one-dimensional model [5,9,16,17,44–47]:

$$\rho c\frac{\partial T}{\partial t} = k\frac{\partial^2 T}{\partial x^2} + \rho q\frac{\partial \alpha}{\partial t} \quad (5)$$

where x is the coordinate along the thickness of the film – see Fig. 3. The temperature and the degree of transformation are functions of time and position, $T(x,t)$ and $\alpha(x,t)$.

According to the isoconversional approach, the evolution of the curing reaction is given by:

$$\frac{\partial \alpha}{\partial t} = A_{\alpha}f(\alpha)\exp\left[-\frac{E_{\alpha}}{R_G T_{\alpha}}\right] \quad (6)$$

where E_α and $A_\alpha f(\alpha)$ are determined by interpolation from discretised set of data E_j and $Af(\alpha)|_j$ that have been obtained from the Friedman isoconversional analysis, Fig. 2.b. That is, we use the result of the Friedman isoconversional analysis to calculate the evolution of the curing reaction.

For the boundary conditions, we considered that one side of the laminate is in perfect thermal contact with the mould, while on the other side heat transport is governed by thermal convection since at the typical curing temperature the contribution of thermal radiation is negligible:

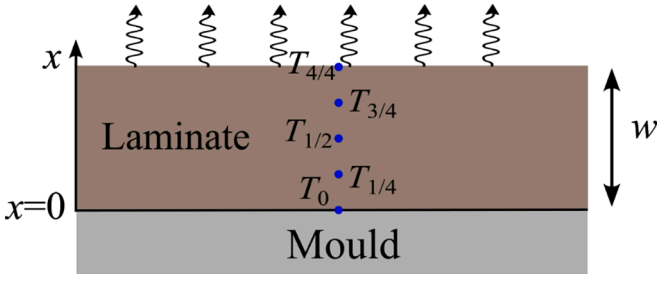

Fig. 3. Schematic representation of the geometry of the model.

$$T(w) = T_m, k\frac{\partial T}{\partial x}\bigg|_{x=0} = h(T(0) - T_m) \tag{7}$$

where w ($0 \le x \le w$) is the laminate thickness, and T_m is the mould temperature. These boundary conditions also cover the case of perfect insulation ($h = 0$), as well as perfect thermal contact on both sides since, by symmetry, the condition $T(0) = T_m$ is equivalent to $\frac{\partial \alpha}{\partial t}\Big|_{x=0} = 0$ for a laminate of thickness $2w$ ($-w \le x \le w$).

Eqs 5–7 can be rearranged in a dimensionless form; something which has been successfully employed to analyse the critical condition for a thermal runaway [48–50], Eq. 8:

$$\frac{\partial \theta}{\partial \tau} = \frac{\partial^2 \theta}{\partial \chi^2} + \theta_T \frac{\partial \alpha}{\partial \tau}, \frac{\partial \alpha}{\partial \tau} = \frac{1}{\theta_T} e^{\frac{\theta}{1+\varepsilon\theta}}, \theta\left(\sqrt{\delta}\right) = 0, \frac{\partial \theta}{\partial \chi}\bigg|_{\chi=0} = \theta(0)\frac{Bi}{\sqrt{\delta}} \tag{8}$$

where $\theta \equiv \frac{E_a}{R}\frac{T-T_m}{T_m^2}$ is the dimensionless temperature, $\tau \equiv t\frac{q}{c}\frac{E_a}{RT_m^2}Ae^{-E_a/RT_m}$ is the dimensionless time and $\chi \equiv x\frac{\sqrt{\delta}}{w}$ the dimensionless coordinate.

Thus, the model is completely described by four dimensionless parameters, viz.: the Arrhenius parameter $\varepsilon \equiv \frac{RT_m}{E_a}$, the Todes parameter $\theta_T \equiv \frac{q}{c}\frac{E_a}{RT_m^2}$, the Frank-Kamenetskii, FK, parameter $\delta \equiv \rho\frac{q}{k}\frac{E_a}{RT_m^2}w^2Ae^{-E_a/RT_m}$ and the Biot number $Bi \equiv h\frac{w}{k}$.

To numerically simulate the continuum model, we made use of a fully implicit finite differences scheme [51]. We imposed the relative error between two iterations to be less that 10^{-14}. We use a spatial grid of 1000 equal-width intervals. Fully implicit schemes are known to be accurate, fast and stable. The latter is essential to deal with thermal runaway.

In Fig. 4, we have plotted the result of a numerical integration using the physical parameters summarized in Table 2 for a 27 mm thick laminate, which was initially thermalized at 20 °C and subsequently, the mould temperature set at 80 °C. We have also plotted the evolution of the temperature at the positions indicated in Fig. 3. For comparison, in Fig. 4 we have represented the measured evolution of the temperatures at the selected positions indicated in Fig. 1 for a 27 mm thick laminate and a furnace temperature of 80 °C. From Fig. 4 we can see that the numerical simulation was able to obtain a maximum overheating that agrees with the experimental one: i.e., the principal objective of this model. Table 2 also provides evidence of the agreement between the calculated and experimental overheating, with a standard deviation between the measured overheat and the corresponding numerical simulations of 3.2 °C for the nine experiments. In the supplementary material (Figs. S7-S15) we have also plotted the nine measured evolutions as well as the related numerical simulations.

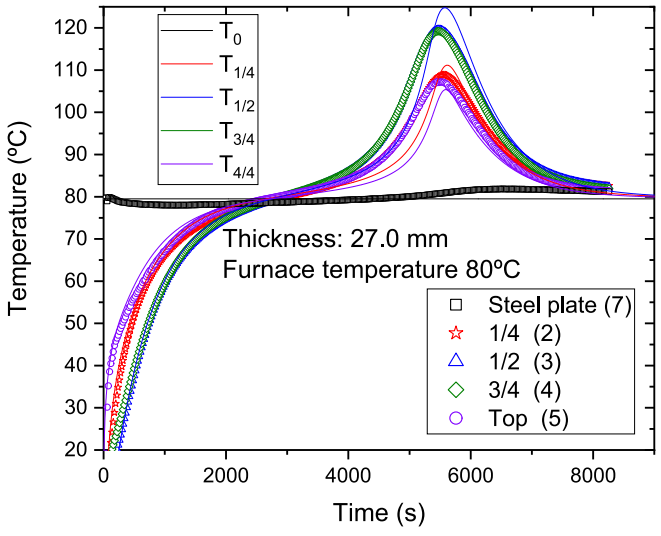

Fig. 4. Solid lines: numerical evolution of the temperature (integration of Eqs. 5–7) at the positions identified in Fig. 3. The physical parameters used in the integration are summarized in Table 2 and for a thickness of 27 mm and a mould temperature of 80 °C. Symbols: evolution of the temperature measured experimentally during the curing process of a 27 mm thick laminate when the oven temperature is 80 °C. The position and the labels of the thermocouples (see Fig. 1) are indicated in the legend.

3. The analytical model

Beyond a critical thickness, heat dissipation cannot compensate heat generation, and the reaction becomes unstable, resulting in thermal runaway. Below this critical thickness, a thermal gradient is formed so that heat dissipation is equal to heat generation and the system reaches a steady state: the so-called subcritical state [48,49]. The maximum temperature difference related to this thermal gradient depends on the thickness of the panel. In this section we determine the critical thickness, w_c, related to a given overheat, $\Delta T_{Max} = T_{Max} - T_m$, as well as the maximum overheat before the steady state becomes unstable.

3.1. Critical thickness related to a given overheat, w_c

Determining the thickness related to a given overheating, ΔT_{Max}, is reduced to determining the dependence of the critical FK parameter, δ_c, as a function of ε, θ_T, Bi and $\theta_{Max} = \frac{\Delta T_{Max}}{\varepsilon T_m}$.

To develop the analytical model we have assumed a constant activation and preexponential term [20]:

$$\frac{\partial \alpha}{\partial t} = Ae^{-E_a/RT} \tag{9}$$

It should be noted that the choice of the particular model is not essential because the critical condition occurs for a rather narrow interval of α.

To determine the constant activation energy and pre-exponential factor, we have taken the average values of E_a and $A_\alpha f(\alpha)$ in the α range from 0.1 to 0.4. We have obtained an activation energy of 88.4 kJ/mol and a pre-exponential factor of 1.0×10^9 s^{-1}. It should be noted that these values are very similar to those obtained for another prepreg having the same epoxy resin VTC401 [25].

In practical conditions, the maximum allowable overheat should be below 20 K, $\Delta T_{Max} \le 20$K, and, since T_m is typically between 400 and 500 K, then $\varepsilon\theta$ will typically be below 0.05, so to develop the analytical model we consider that $\varepsilon\theta \ll 1$. To check the validity of this approximation we perform numerical calculations for different values of ε and compare the numerical and analytical analysis.

Besides this, to separate the contribution of the different parameters, we first consider the limiting case of highly exothermic reactions (infinite Todes parameter) and perfect upper insulation ($Bi = 0$). Then, we develop a second model that considers finite Todes values, and finally, a general model that also takes into account convective heat losses.

Case a) Highly exothermic reaction: $\theta_T \to \infty$, $\varepsilon\theta \ll 1$ and $Bi = 0$

If we assume $\theta_T \to \infty$, and perfect thermal insulation at the top side ($Bi = 0$), Eq. 8 reduces to Eq. 9:

$$\frac{\partial \theta}{\partial \tau} = \frac{\partial^2 \theta}{\partial \chi^2} + e^{\theta}, \theta\left(\sqrt{\delta}\right) = 0, \frac{\partial \theta}{\partial \chi}\bigg|_{\chi=0} = 0 \tag{9}$$

Eq. 9 has an exact analytical solution for the stationary state, $\frac{\partial \theta}{\partial \tau} = 0$ [42,50]:

$$\theta = 2\ln\left[C_2 \operatorname{sech}\left(\frac{C_2}{\sqrt{2}}(\chi + C_1)\right)\right] \tag{10}$$

where C_1 and C_2 are integration constants to be determined from the two boundary conditions. Note that the maximum temperature corre-

sponds to $\mathrm{sech}\left(\frac{C_2}{\sqrt{2}}(\chi + C_1)\right) = 1$, thus $C_2 = e^{\theta_{Max}/2}$. Besides, from the condition $\left.\frac{\partial\theta}{\partial\chi}\right|_{\chi=0} = 0$ the maximum being located at $\chi = 0$ can be obtained, thus $C_1 = 0$. Therefore, the stationary solution is:

$$\theta = 2\ln\left[e^{\theta_{Max}/2}\mathrm{sech}\left(\frac{e^{\theta_{Max}/2}}{\sqrt{2}}\chi\right)\right], \tag{11}$$

In Fig. 5 we have plotted the temperature profile for $\theta_{Max} = 0.329$. It can be seen that the temperature increases steadily from the side that is in thermal contact with the mould ($\chi = \sqrt{\delta}$) to the insulated side ($\chi = 0$).

Finally, the critical condition is obtained after imposing the boundary condition $\theta\left(\sqrt{\delta}\right) = 0$:

$$\delta_{c,\infty,0,0} = 2e^{-\theta_{Max}}\mathrm{arcosh}^2\left(e^{\theta_{Max}/2}\right), \tag{12}$$

where the subscripts ∞ and 0 of $\delta_{c,\infty,0,0}$ stand for $\theta_T \to \infty$, $\varepsilon = 0$ and $Bi = 0$. In Fig. 6 we compare the critical value of the FK parameter determined from the analytical model (Eq. 12), and by numeric integration of the continuous model. The numerical data is obtained from the integration of Eq. 8 with $\theta_T = 10^6$, $\varepsilon = 0.004$, $Bi = 0$ and $0.01 \le \delta \le 0.8833$. The agreement between the analytical solution and the numerical simulations is remarkable; the deviations are mainly related to the fact that the Todes parameter has a finite value.

To determine the dependence of the critical thickness on ε, we have integrated Eq. 8 for different values of ε and θ_{Max} in the limit of $\theta_T \to \infty$; the result is shown in Fig. 7.a. Each point in Fig. 7.a is obtained by fixing the value of ε and determining the value of FK parameter related to the given θ_{Max} overheating. Afterwards, we have performed a non-linear fit. From the non-linear fit we can obtain the critical value $\delta_{c,\infty,0,0}$, and subsequently, the critical thickness from the definition of the FK parameter,

$$w_{c,\infty,0} = \sqrt{\delta_{c,\infty,0,0}(1 + 0.72\varepsilon\theta_{Max}^2)\frac{a}{A}\frac{1}{\theta_T}e^{1/\varepsilon}} \tag{13}$$

where $a = k/(\rho c)$ is the thermal diffusivity.

Case b) Moderate exothermal. Finite values of θ_T.

To determine the critical thickness for finite values of θ_T and $Bi = 0$, $w_{c,0}$, we have integrated Eq. 8 for different values of θ_T and θ_{Max}; the result of which is shown in Fig. 7.b. Each point in Fig. 7 is obtained by

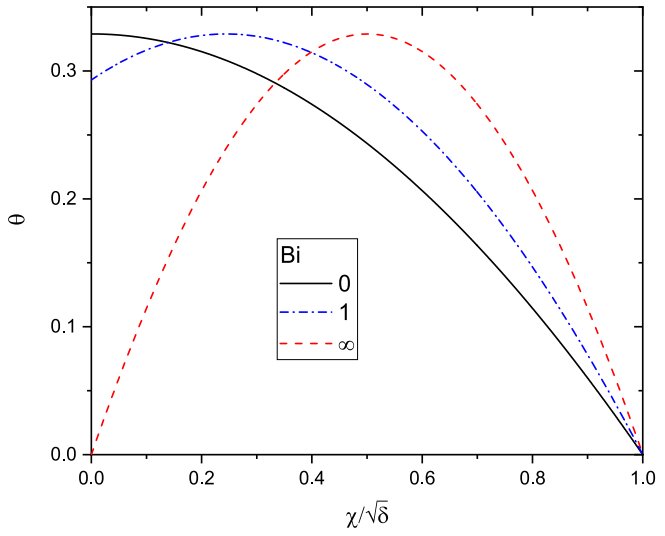

Fig. 5. Stationary temperature profiles, Eq. 11, for different values of Biot parameter, $\theta_{Max} = 0.329$ and $\delta_{c,0} = 0.5$.

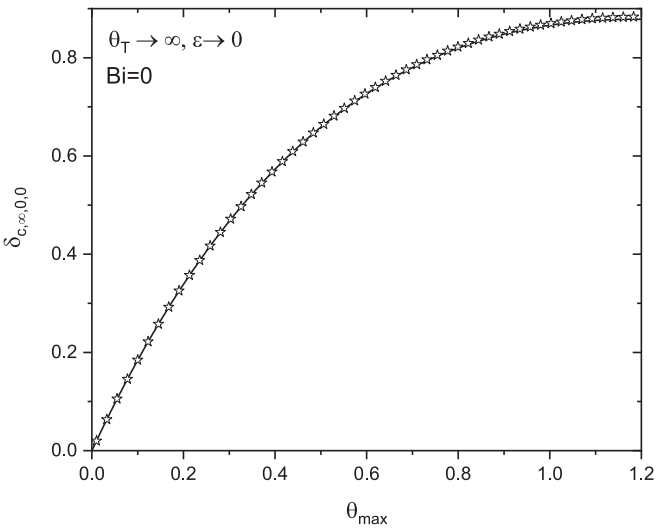

Fig. 6. Critical value of the FK parameter as a function of the dimensionless overheating. Solid line theoretical prediction for $\theta_T \to \infty$, $\varepsilon = 0$ and $Bi = 0$, Eq. 12. Stars, numerical analysis for $\theta_T = 10^6$, $\varepsilon = 0.004$ and $Bi = 0$.

fixing the values of θ_T and ε, and determining the FK value related to the given θ_{Max} overheating. Once we know the $\delta_{c,0}$ we can easily determine $w_{c,0}$ from the definition of the FK parameter. In total, we have analysed more than 10,000 numerical cases. The numerical analysis covers a large range of parameters: $0.02 \le \theta_T \le 10^6$ and $0.01 \le \theta_{Max} \le 1.1$. We have fitted the numerical data to a power function, so the approximate dependence of the critical thickness on the system parameters for $Bi = 0$ is:

$$w_{c,0} = w_{c,\infty,0}\left[1 + 0.76\left(\frac{\theta_{Max}}{\theta_T}\right)^{3.5-1.4\theta_{Max}}\right] \tag{14}$$

where $w_{c,\infty,0}$ is the critical thickness for $\theta_T \to \infty$ and $Bi = 0$, Eq. 13.

Case c) General solution, $Bi \neq 0$.

In this subsection, we will quantify the effect of not having a perfectly insulating end. In this case, Eq. 10 also holds and $C_2 = e^{\theta_{Max}/2}$ but $C_1 \neq 0$. Indeed C_1 is related to the *Bi* number. When $Bi = 0$, $C_1 = 0$. Moreover, as we have discussed in the previous section, a perfect thermal contact on both sides is equivalent to a laminate of thickness $2w$, then for $Bi = \infty$, $C_1 = -\sqrt{\delta}/2$. Thus $-\frac{\sqrt{\delta}}{2} < C_1 < 0$. Furthermore, as can be seen in Fig. 5, the position at which the temperature reaches its maximum depends on *Bi*: $\chi_{Max} = -C_1$, thus it shifts from the insulated end when $Bi = 0$ to the center of the laminate when $Bi = \infty$.

To determine the dependence of the analytical solution on the *Bi* number and on θ_{Max} we have determined C_1 in Eq. 10 by imposing the general boundary conditions, Eq. 9. We considered four values of θ_{Max}: 0.24, 0.6, 0.8 and 1.1, which cover most of the achievable range of values ($0 < \theta_{Max} < 1.19$). As for the *Bi* number, we have taken the range from 0.001 to 1000; the result is shown in Fig. 8. As noted earlier, by symmetry, the case of a perfect thermal contact is equivalent to an insulating boundary of a double-thickness laminate, therefore the ratio between the critical thickness, w_c, and the critical thickness for the same parameters but with $Bi = 0$, $w_c/w_{c,0}$, evolves from 1 when $Bi = 0$ to 2 for $Bi = \infty$. Moreover, Fig. 8 shows that the dependence of $w_c/w_{c,0}$ on θ_{Max} is negligible, so we can fit this dependence to a function that depends only on $Bi\frac{w_{c,0}}{w}$:

$$w_c = w_{c,0}\left[2 - \left(1 + 0.63\left[h\frac{w_{c,0}}{k}\right]^{1.2}\right)^{-1}\right] \tag{15}$$

where $w_{c,0}$ is the critical thickness for $Bi = 0$, Eq. 14.

Notice that in Fig. 8 and Eq. 15, we have taken a different

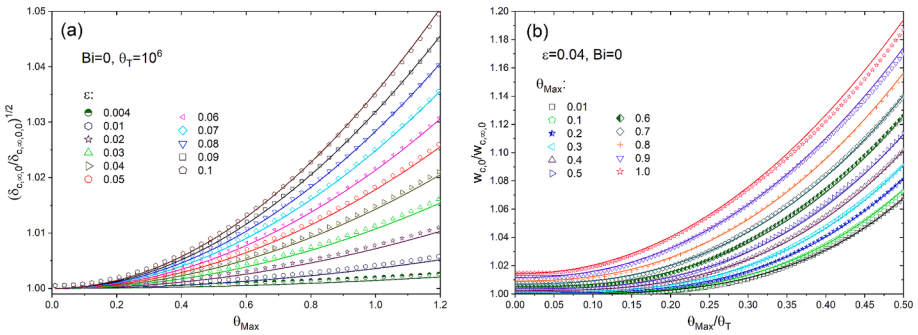

Fig. 7. (a) $\delta_{c,\infty,0,0}$ symbols: $\sqrt{\delta_{c,\infty,0}/\delta_{c,\infty,0,0}}$ determined from numerical simulations for $\theta_T = 10^6$ and different values of θ_{Max} and ε: $0.01 \le \theta_{Max} \le 1.19$ and $0.004 \le \varepsilon \le 0.1$. Solid line: non-linear fit. (b) Symbols: critical thickness determined from numerical simulations for $\varepsilon = 0.04$ and different values of θ_T and θ_{Max}: $0.02 \le \theta_T \le 10^6$ and $0.01 \le \theta_{Max} \le 1.1$. Solid line: non-linear fit, Eq. 14.

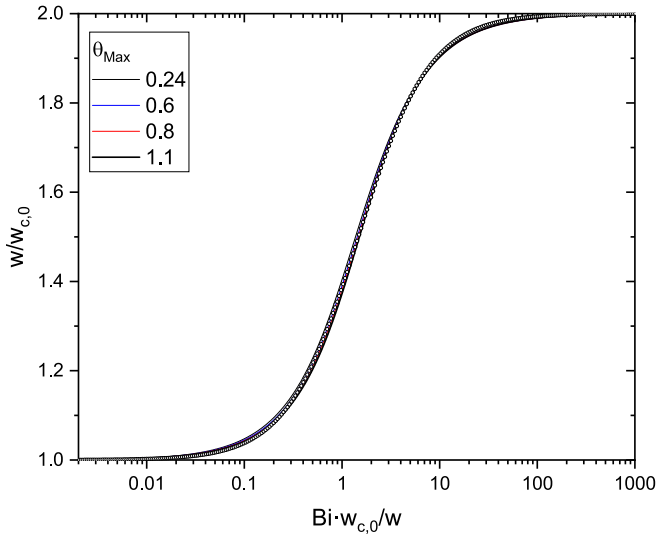

Fig. 8. Lines: theoretical critical thickness as a function of the *Bi* number for different values of the temperature overheat, θ_{Max}. Symbols: fitted solution, Eq. 15.

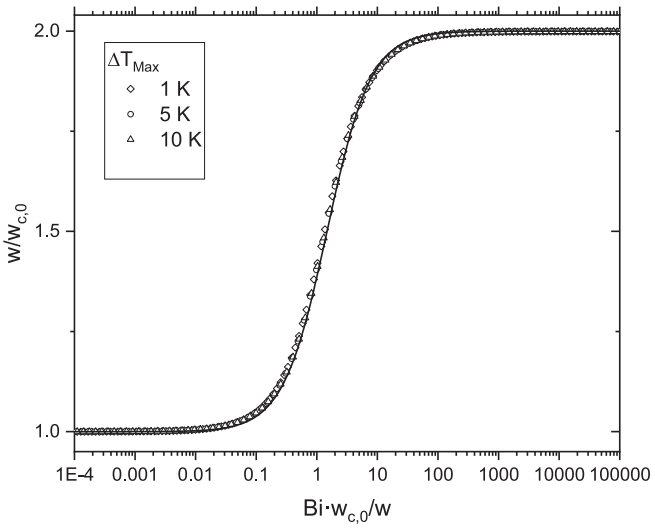

Fig. 9. Symbols: critical thickness determined from numerical simulations and for three different temperature overheats. Line: analytical solution Eq. 15.

dimensionless parameter $Bi\frac{w_{c,0}}{w} = h\frac{w_{c,0}}{k}$ instead of taking the number *Bi* as a parameter. The reason for this is to simplify the critical thickness calculation. If we had used the number *Bi* instead of $h\frac{w_{c,0}}{k}$, determining w_c would have been more complex because the number *Bi* also depends on w_c, so that the two terms on both sides of the equality depend on w_c. In contrast, using $h\frac{w_{c,0}}{k}$ as a parameter allows us to determine w_c directly from Eq. 15.

To check the validity of Eq. 15, we calculated numerically the ratio $w_c/w_{c,0}$ for a Todes parameter $\theta_T = 6.486$ and for three different overheating values. The results are plotted in Fig. 9, confirming a perfect agreement between Eq. 15 and the numerical analysis despite the fact that the numerical data has been obtained for a θ_T far from the condition $\theta_T \to \infty$. Consequently, the validity of Eq. 15 goes beyond the limit case $\theta_T \to \infty$.

3.2. Critical thickness for a thermal runaway, w_{TR}

Fig. 6 shows that for the limit case $\theta_T \to \infty$ there is a maximum FK parameter value of $\delta_{TR,\infty} = 0.878458$, i.e., for FK parameter values above this maximum there is no solution for the subcritical steady state. This means that for $\delta > \delta_{TR,\infty}$ the system becomes unstable and it undergoes a thermal runaway (the subscript *TR* stands for thermal runaway). This value is the well-known critical FK parameter [52] that is related to a critical thickness, $w_{TR,\infty}$:

$$w_{TR,\infty} = \sqrt{0.878(1 + 0.72\varepsilon\theta_{Max}^2)\frac{a}{A}\frac{1}{\theta_T}e^{1/\varepsilon}} \tag{16}$$

For thicknesses above $w_{TR,\infty}$, i.e., for $\delta > \delta_{TR,\infty}$, the reaction becomes unstable, and the system undergoes a thermal runaway.

This critical FK parameter value is related to a critical overheat, $\theta_{Max,TR} = 1.19$, see Fig. 6. This means that there is a maximum overheat above which the system becomes unstable, and the temperature increase approaches the adiabatic one. From the definition of the dimensionless temperature, we can determine this maximum overheat, $\Delta T_{Max,TR}$:

$$\Delta T_{Max,TR} = 1.19\frac{RT_m^2}{E_a} \tag{17}$$

For example, for a mould temperature of 500 K and an activation energy of 100 kJ/mol, the maximum overheat is 24.7 K. In other words, if during the curing process the local overheat exceeds 24.7 K, the reaction becomes unstable, and the temperature suddenly rises to a much higher overheat. Note, that in reference [20] parameter β corresponds to the FK parameter, thus the critical condition developed in ref. [20] is equivalent to Eq. 16, i.e., our limit condition for the limit case $\theta_T \to \infty$.

The critical values of $\delta_{TR,\infty}$ and $w_{TR,\infty}$ correspond to the limit case $\theta_T \to \infty$. To determine the critical thickness for finite values of Todes parameter, w_{TR}, we have used Eq. 14 but replaced θ_{Max} with $\theta_{Max,TR}$:

$$w_{TR,0} = w_{TR,\infty}\left[1 + 0.76\left(\frac{1.19}{\theta_T}\right)^{1.8}\right] \quad (18)$$

Finally, to determine the critical thickness for $Bi \neq 0$ we use Eq. 15:

$$w_{TR} = w_{TR,0}\left[2 - \left(1 + 0.63\left[h\frac{w_{TR,0}}{k}\right]^{1.2}\right)^{-1}\right] \quad (19)$$

To check the validity of our solution, we used Eq. 18 to determine δ_{TR} as a function of Todes parameter and compare it to the most relevant models available in the literature [42,53–57], the result of which is shown in Fig. 10. Note that all models show a perfect agreement when $\theta_T \to \infty$ but the differences between the models are significant for finite values of Todes parameter. The reason for this is that these models have been developed for explosive or highly energetic materials, i.e., the reactions analysed by these models exhibit large values of Todes parameter. However, in the case of the curing reaction of resins or prepregs, the values of the Todes parameter are quite low. For instance, typical values for an epoxy resin are: q between 30×10^5 and 50×10^5 J/kg, c is between 1000 and 1500 J/(kg·K), E_a is between 50 and 80 kJ/mol and curing temperatures are between 300 and 400 K [34,58–61]. Thus, the Todes parameter for resins is generally well below 50 ($1/\theta_T > 0.02$). In the case of prepregs, the presence of the carbon fibre significantly reduces the specific heat of reaction, and so the value of the Todes parameter is lower than that of the resin [7]. For instance, in our case (Table 2) the Todes parameter ranges from 9 to 12.5 in the temperature interval from 60 to 120 °C. From Fig. 10 it is clear that our model and that of Gebart [20] are the ones that best predict the numerical data. Indeed, both models have been developed to deal with the occurrence of thermal runaway during the curing reactions, however, our model has the advantage that it also takes into account convection losses and non-zero Arrhenius values, while Gebart's model assumes $\varepsilon = 0$ and $Bi = 0$. Finally, from the agreement between our analytical model and the numerical simulation, we observed that the analytical solution covers a wide range of parameters ranging from highly energetic materials to the curing process of an epoxy resin.

4. Experimental validation

Once the analytical solution had been developed, we are now able to construct a transformation map relating the curing temperature to the critical thickness for different overheating and for thermal runaway. The result for the physical parameters of the laminates used in the experiments (Table 2) is shown in Fig. 11. In the supplementary material, we have included the Matlab/Octave code used to build this map (Table S2). In addition, in Fig. 11 we have indicated curing temperature, film thickness, and the measured overheating for the nine experiments performed (see Table 1). From Fig. 11, a perfect agreement between the predicted and measured overheating – within the experimental accuracy – can be confirmed.

We have also constructed this map for a different system (supplementary material, Fig. S16), and again we have obtained a good agreement between our numerical prediction and the numerical simulations reported in [7].

5. Conclusions

In the present work, a simple 1D model to determine the formation of thermal gradients within a planar geometry sample during the isothermal curing process of an epoxy resin was developed. The model considers the heat generated by the curing process, the heat dissipated through the sample, and different boundary conditions: perfect conduction on one side and convective losses on the other.

Due to the simplicity of the reaction model, this model is not able to accurately predict the course of the curing reaction, but it is able to accurately determine the overheating.

From the model, we have developed analytical equations able to predict the critical thickness to reach a given overheating or thermal runaway. The analytical equations and the numerical integration of the model show a remarkable agreement. This analytical approach reveals the dependence of this critical thickness on the physical parameters: curing temperature, thermal conductivity, specific heat capacity, apparent convective coefficient, density, specific heat of reaction, activation energy and pre-exponential factor.

The numerical and analytical models have been checked against experimental data. In total, nine experiments were carried out with laminates made from a commercial prepreg. Different laminate thicknesses and curing temperatures have been analysed. The results show a good agreement between the experimental data, the numerical analysis

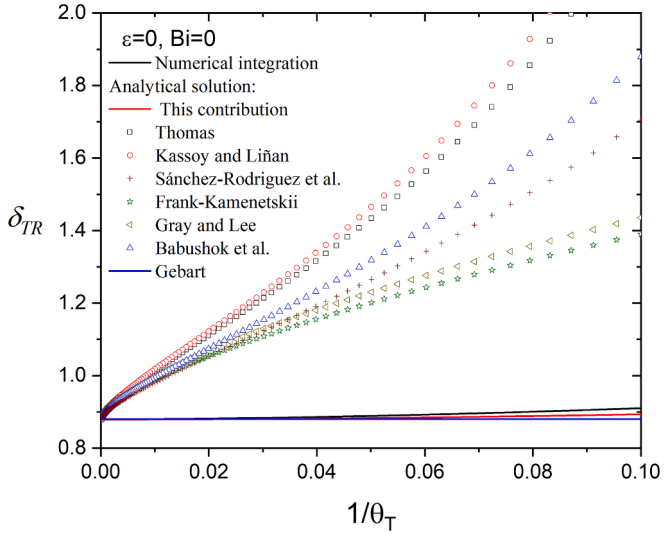

Fig. 10. Red solid line: dependence of δ_{TR} on Todes parameter, Eq. 14. Black solid line dependence obtained numerically from the integration of Eq. 8 imposing $\theta_{Max} = 1.19$. Symbols analytical predictions of Thomas [53], Frank-Kamenetskii [55], Kassoy and Liñan [54], Gray and Lee [56], Babushok et al. [57], Sánchez-Rodríguez et al. [42] and blue line Gebart [20].

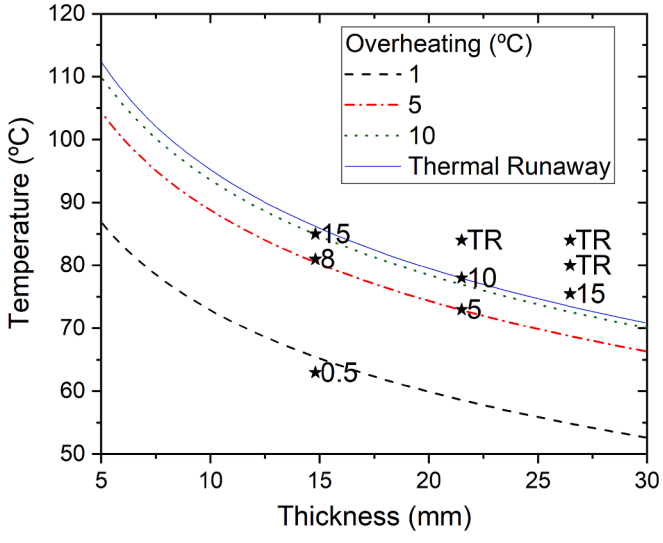

Fig. 11. Lines: analytical prediction of the curing temperatures to reach a given overheating, Eqs. 14 and 15, or thermal runaway, Eqs. 18 and 19, as a function of the laminate thickness. Table 2 shows the physical parameters used in the analytical prediction. The stars indicate curing temperature and thickness for the experiments summarized in Table 1. The label attached to the symbol indicates the observed overheating.

and the analytical model.

The analytical model has been used to construct a thickness-temperature diagram to determine overheating and whether or not thermal runaway will occur, as a function of curing temperature and sample thickness.

The agreement between numerical simulations and analytical prediction covers a wide range of parameters, from highly energetic materials to the curing process of an epoxy resin, so it can be applied to a wide variety of systems.

CRediT authorship contribution statement

Jordi Farjas: Writing – review & editing, Writing – original draft, Software, Methodology, Investigation, Formal analysis, Conceptualization. **Daniel Sanchez-Rodriguez:** Writing – review & editing, Supervision, Investigation, Data curation, Conceptualization. **Sihem Zaidi:** Investigation, Formal analysis, Data curation. **Didina-Ramona-Casandra Cârstea:** Validation, Investigation, Formal analysis, Data curation. **Ahmed Mohamed Saleh Abd Elfatah:** Investigation, Formal analysis, Data curation. **Andrei Rotaru:** Writing – review & editing, Supervision, Methodology, Investigation, Conceptualization. **Josep Costa:** Writing – review & editing, Supervision, Methodology, Investigation, Funding acquisition, Conceptualization.

Declaration of competing interest

The authors declare the following financial interests/personal relationships which may be considered as potential competing interests: Josep Costa reports financial support was provided by Spain Ministry of Science and Innovation. Daniel Sanchez-Rodriguez reports financial support was provided by Generalitat de Catalunya Ministry of Research and Universities. If there are other authors, they declare that they have no known competing financial interests or personal relationships that could have appeared to influence the work reported in this paper.

Acknowledgements

The authors acknowledge AMADE and the GRMT project (PID2021-126989OB-I00 financed by the MCI, Spain). We also thank the Catalan Government's support with 2017SGR1378. D.S.R. acknowledges the support received from the Beatriu de Pinós Programme, and the Ministry of Research and Universities of the Government of Catalonia (Fellowship BP00069).

Appendix A. One-dimensional heat flow criterion

To establish a bound on the width to thickness ratio for the validity of the hypothesis that heat flows in the thickness direction, we consider that heat flow results from the parallel combination of two different paths: the transverse path and the in-plane path. The time required for heat to dissipate by thermal conduction is proportional to the square of the path length divided by the thermal diffusivity. Thus, for the in-plane direction

$$t_l \propto \frac{l^2}{a_l}$$

where l is the width of the sample and a_l is the thermal diffusivity, $a_l = k_l/(\rho c)$, and k_l is the thermal conductivity in the in-plane direction. Likewise, for the transverse direction:

$$t_t \propto \frac{w^2}{a_t}$$

where w is the thickness of the sample and a_t is the thermal diffusivity, $a_t = k_t/(\rho c)$, and k_t is the thermal conductivity in the transverse direction. The heat flow through the in-plane direction will be negligible if the time required for the heat to dissipate through the in-plane direction is much greater than through the transverse direction:

$$\frac{l^2}{a_l} \gg \frac{w^2}{a_t}$$

Thus, the condition for the width to thickness ratio is:

$$\left(\frac{l}{w}\right)^2 \frac{a_t}{a_l} \gg 1$$

In our case, for the thickest panel we have a ratio $\frac{l}{w} = 4$ and if we assume that for a prepreg made of carbon fibres the thermal conductivity in the in-plane direction is three times that of the transverse direction [7], the condition becomes:

$$\left(\frac{l}{w}\right)^2 \frac{a_t}{a_l} \simeq 5$$

For the thickest panel the condition is satisfied but we approach the bound. In case the heat dissipated through the in-plane direction is not negligible, the heat accumulated in the central region will be lower than that predicted by the one dimensional model, and therefore the actual overheating will be lower than that obtained from the simulated data using the one dimensional model. From the comparison between numeric simulations and experimental results (Figs. S13-S15), and within the data dispersion, we cannot asses a tendency to lower overheating for the experimental data. Thus, the contribution of the heat transport through the in-plane direction is smaller than the experimental inaccuracies.

Appendix B. Supplementary data

Supplementary data to this article can be found online at https://doi.org/10.1016/j.compositesa.2025.108815.

Data availability

Data will be made available on request.

References

[1] Halm D, Fouillen F, Lainé E, Gueguen M, Bertheau D, van Eekelen T. Composite pressure vessels for hydrogen storage in fire conditions: Fire tests and burst simulation. Int J Hydrogen Energy 2017;42:20056–70. https://doi.org/10.1016/j.ijhydene.2017.06.088.

[2] Breen C, Guild F, Pavier M. Impact of thick CFRP laminates: The effect of impact velocity, in: Compos Part A Appl Sci Manuf, Elsevier Ltd, 2005: pp. 205–211. doi: 10.1016/j.compositesa.2004.06.005.

[3] Zimmermann K, Zenkert D, Siemetzki M. Testing and analysis of ultra thick composites. Compos B Eng 2010;41:326–36. https://doi.org/10.1016/j.compositesb.2009.12.004.

[4] Hoffmann M, Zimmermann K, Bautz B, Middendorf P. A new specimen geometry to determine the through-thickness tensile strength of composite laminates. Compos B Eng 2015;77:145–52. https://doi.org/10.1016/j.compositesb.2015.03.020.

[5] Gorovaya TA, Korotkov VN. Quick cure of thermosetting composites. Compos Part A Appl Sci Manuf 1996;27:953–60. https://doi.org/10.1016/1359-835X(96)00055-3.

[6] Lorenz N, Müller-Pabel M, Gerritzen J, Müller J, Gröger B, Schneider D, et al. Characterization and modeling cure- and pressure-dependent thermo-mechanical and shrinkage behavior of fast curing epoxy resins. Polym Test 2022;108:107498. https://doi.org/10.1016/j.polymertesting.2022.107498.

[7] Esposito L, Sorrentino L, Penta F, Bellini C. Effect of curing overheating on interlaminar shear strength and its modelling in thick FRP laminates. Int J Adv Manuf Technol 2016;87:2213–20. https://doi.org/10.1007/s00170-016-8613-5.

[8] Ciriscioli PR, Qiuling Wang. G.S. Springer, autoclave curing — comparisons of model and test results. J Compos Mater 1992;26:90–102. https://doi.org/10.1177/002199839202600106.

[9] Twardowski TE, Lin SE, Geil PH. Curing in thick composite laminates: experiment and simulation. J Compos Mater 1993;27:216–50. https://doi.org/10.1177/002199839302700301.

[10] Bogetti TA, Gillespie JW. Two-dimensional cure simulation of thick thermosetting composites. J Compos Mater 1991;25:239–73. https://doi.org/10.1177/002199839102500302.

[11] Dai SC, Ye L. Characteristics of CF/PEI tape winding process with on-line consolidation. Compos Part A Appl Sci Manuf 2002;33:1227–38. https://doi.org/10.1016/S1359-835X(02)00083-0.

[12] Sorrentino L, Esposito L, Bellini C. A new methodology to evaluate the influence of curing overheating on the mechanical properties of thick FRP laminates. Compos B Eng 2017;109:187–96. https://doi.org/10.1016/j.compositesb.2016.10.064.

[13] Oh JH, Lee DG. Cure cycle for thick glass/epoxy composite laminates. J Compos Mater 2002;36:19–45. https://doi.org/10.1177/0021998302036001300.

[14] Tifkitsis KI, Mesogitis TS, Struzziero G, Skordos AA. Stochastic multi-objective optimisation of the cure process of thick laminates. Compos Part A Appl Sci Manuf 2018;112:383–94. https://doi.org/10.1016/j.compositesa.2018.06.015.

[15] Dolkun D, Zhu W, Xu Q, Ke Y. Optimization of cure profile for thick composite parts based on finite element analysis and genetic algorithm. J Compos Mater 2018;52:3885–94. https://doi.org/10.1177/0021998318771458.

[16] Voto G, Sequeira L, Skordos AA. Heating rate limits in fast cure processing of thick carbon fibre laminates. ECCM 2018–18th European Conference on Composite Materials 2019:24–8.

[17] Ruiz E, Trochu F. Numerical analysis of cure temperature and internal stresses in thin and thick RTM parts. Compos Part A Appl Sci Manuf 2005;36:806–26. https://doi.org/10.1016/j.compositesa.2004.10.021.

[18] Keller A, Dransfeld C, Masania K. Flow and heat transfer during compression resin transfer moulding of highly reactive epoxies. Compos B Eng 2018;153:167–75. https://doi.org/10.1016/j.compositesb.2018.07.041.

[19] Leistner C, Hartmann S, Abliz D, Ziegmann G. Modeling and simulation of the curing process of epoxy resins using finite elements. Contin Mech Thermodyn 2020;32:327–50. https://doi.org/10.1007/s00161-018-0708-9.

[20] Gebart R. Thermal runaway criterion for thick polymer composites. Compos Part A Appl Sci Manuf 2024;182:108187. https://doi.org/10.1016/j.compositesa.2024.108187.

[21] Roura P, Sanchez-Rodriguez D, Farjas J. Measurement by differential scanning calorimetry of specific heat capacity variation due to crystallization: Application to amorphous silicon. Thermochim Acta 2011;522:161–5. https://doi.org/10.1016/j.tca.2011.02.014.

[22] Zghal I, Farjas J, Camps J, Dammak M, Roura-Grabulosa P. Thermal decomposition of cerium triethanolamine complexes. Thermochim Acta 2020;683:178430. https://doi.org/10.1016/j.tca.2019.178430.

[23] Khabari A, Zenouzi M, O`Connor T, Rodas A. Natural and forced convective heat transfer analysis of nanostructured surface. Lecture Notes Eng Comput Sci 2014;1:317–9.

[24] Borchardt HJ, Daniels F. The application of differential thermal analysis to the study of reaction kinetics 1. J Am Chem Soc 1957;79:41–6. https://doi.org/10.1021/ja01558a009.

[25] Menczel JD, Judovits L, Prime RB, Bair HE, Reading M, Swier S. Thermal analysis of polymers. Wiley, Hoboken, NJ, USA 2009. https://doi.org/10.1002/9780470423837.

[26] Brown ME, Maciejewski M, Vyazovkin S, Nomen R, Sempere J, Burnham A, et al. Computational aspects of kinetic analysis: Part A: The ICTAC kinetics project-data, methods and results. Thermochim Acta 2000;355:125–43. https://doi.org/10.1016/S0040-6031(00)00443-3.

[27] Farjas J, Roura P. Isoconversional analysis of solid state transformations. A critical review. Part I. Single step transformations with constant activation energy. J Therm Anal Calorim 105 2011:757–66. https://doi.org/10.1007/s10973-011-1446-4.

[28] Vyazovkin S, Achilias D, Fernandez-Francos X, Galukhin A, Sbirrazzuoli N. ICTAC kinetics committee recommendations for analysis of thermal polymerization kinetics, 714. Thermochim Acta 2022:179243. https://doi.org/10.1016/j.tca.2022.179243.

[29] Wan J, Li C, Bu Z-Y, Xu C-J, Li B-G, Fan H. A comparative study of epoxy resin cured with a linear diamine and a branched polyamine. Chem Eng J 2012;188:160–72. https://doi.org/10.1016/j.cej.2012.01.134.

[30] Granado L, Sbirrazzuoli N. Isoconversional computations for nonisothermal kinetic predictions. Thermochim Acta 2021;697:178859. https://doi.org/10.1016/j.tca.2020.178859.

[31] Hu J, Shan J, Zhao J, Tong Z. Isothermal curing kinetics of a flame retardant epoxy resin containing DOPO investigated by DSC and rheology. Thermochim Acta 2016;632:56–63. https://doi.org/10.1016/j.tca.2016.02.010.

[32] Budrugeac P, Cucos A, Dascălu R, Paraschiv C, Mitrea S, Sbarcea BG. The use of thermal analysis methods for predicting the thermal endurance of an epoxy resin used as electrical insulator. J Therm Anal Calorim 2021;146:1791–801. https://doi.org/10.1007/s10973-020-10156-5.

[33] González Ruiz JA, Farjas J, Blanco N, Costa J, Gascons M. Assessment of unexplored isoconversional methods to predict epoxy-based composite curing under arbitrary thermal histories. J Reinf Plast Compos 2023;42:1067–74. https://doi.org/10.1177/07316844221145591.

[34] Sanchez-Rodriguez D, Zaidi S, Jahani Y, Ruiz de Luzuriaga A, Rekondo A, Maimi P, et al. Processability and reprocessability maps for vitrimers considering thermal degradation and thermal gradients. Polym Degrad Stab 2023;217:110543. https://doi.org/10.1016/j.polymdegradstab.2023.110543.

[35] Zaidi S, Thakur S, Sanchez-Rodriguez D, Verdejo R, Farjas J, Costa J. Optimal processing conditions of a bio-based epoxy synthesized from vanillyl alcohol. Polym Degrad Stab 2024;223:110743. https://doi.org/10.1016/j.polymdegradstab.2024.110743.

[36] Sanchez-Rodriguez D, Zaidi S, Carreras L, Ruiz de Luzuriaga A, Rekondo A, Costa J, et al. Time-temperature-transformation diagrams from isoconversional kinetic analyses applied to the processing and reprocessing of vitrimers. Thermochim Acta 2024;736:179744. https://doi.org/10.1016/j.tca.2024.179744.

[37] Vyazovkin S. Isoconversional kinetics of polymers: the decade past. Macromol Rapid Commun 2017;38:1600615. https://doi.org/10.1002/marc.201600615.

[38] Vyazovkin S, Sbirrazzuoli N. Isoconversional methods as single-step kinetic approximation. Thermochim Acta 2024;733:179692. https://doi.org/10.1016/j.tca.2024.179692.

[39] Friedman HL. Kinetics of thermal degradation of char-forming plastics from thermogravimetry. Application to a phenolic plastic. J Polym Sci Part C: Polym Symposia 1964;6:183–95. https://doi.org/10.1002/polc.5070060121.

[40] Vyazovkin S, Sbirrazzuoli N. Isoconversional kinetic analysis of thermally stimulated processes in polymers. Macromol Rapid Commun 2006;27:1515–32. https://doi.org/10.1002/marc.200600404.

[41] Farjas J, Roura P. Isoconversional analysis of solid-state transformations. A critical review. Part III. Isothermal and non isothermal predictions. J Therm Anal Calorim 109 2012:183–91. https://doi.org/10.1007/s10973-011-1642-2.

[42] Sánchez-Rodriguez D, Farjas J, Roura P. The critical condition for thermal explosion in an isoperibolic system. AIChE J 2017;63:3979–93. https://doi.org/10.1002/aic.15727.

[43] Ren M, Wang Q, Cong J, Chang X. Study of one-dimensional cure simulation applicable conditions for thick laminates and its comparison with three-dimensional simulation. IEEE J Sel Top Quantum Electron 2018;25:1197–204. https://doi.org/10.1515/secm-2017-0244.

[44] Gebart BR. Critical parameters for heat transfer and chemical reactions in thermosetting materials. J Appl Polym Sci 1994;51:153–68. https://doi.org/10.1002/app.1994.070510116.

[45] Capehart TW, Kia HG, Abujoudeh T. Cure simulation of thermoset composite panels. J Compos Mater 2007;41:1339–60. https://doi.org/10.1177/0021998306068077.

[46] Frulloni E, Salinas MM, Torre L, Mariani A, Kenny JM. Numerical modeling and experimental study of the frontal polymerization of the diglycidyl ether of bisphenol a/diethylenetriamine epoxy system. J Appl Polym Sci 2005;96:1756–66. https://doi.org/10.1002/app.21644.

[47] Young W-B. Compacting pressure and cure cycle for processing of thick composite laminates. Compos Sci Technol 1995;54:299–306. https://doi.org/10.1016/0266-3538(95)00067-4.

[48] Frank-Kamenetskii DA. Diffusion and Heat Exchange in Chemical Kinetics. 2nd ed. New Jersey: Princeton University Press; 1955.

[49] Merzhanov AG, Averson AEE. The present state of the thermal ignition theory: An invited review. Combust Flame 1971;16:89–124. https://doi.org/10.1016/S0010-2180(71)80015-9.

[50] Gill W, Donaldson AB, Shouman AR. The Frank-Kamenetskii problem revisited. Part I. Boundary conditions of first kind. Combust Flame 1979;36:217–32. https://doi.org/10.1016/0010-2180(79)90061-0.

[51] Press WH, Flannery BP, Teukolsky SA, Vetterling WT. Numerical recipes in C: the art of scientific computing. Cambridge: Cambridge University Press; 1994.

[52] Semenov N. Thermal theory of combustion and explosion. Progress of Physical Science USSR 1940;23:251–92.
[53] Thomas PH, Bowes PC. Some aspects of the self-heating and ignition of solid cellulosic materials. Br J Appl Phys 1961;12:222–9. https://doi.org/10.1088/0508-3443/12/5/305.
[54] Kassoy DR, Liñan A. The influence of reactant consumption on the critical conditions for homogeneous thermal explosions. Q J Mech Appl Math 1978;31:99–112. https://doi.org/10.1093/qjmam/31.1.99.
[55] Frank-Kamenetskii DA. Nonstationary theory of thermal explosion. Zh. Fiz Khim (J Phys Chem USSR) 1946;20:139–44.
[56] Gray P, Lee PR. Thermal explosion theory. In: Tipper C, editor. Oxidation and Combustion Reviews, Vol 2. Amsterdam: Elsevier; 1967. p. 1–184.
[57] Babushok VI, Goldshtein VM, Sobolev VA. Critical conditions for thermal explosion with reactant consumption. Combust Sci Technol 1990;70:81–9. https://doi.org/10.1080/00102209008951613.
[58] Santiago D, Fernández-Francos X, Ramis X, Salla JM, Sangermano M. Comparative curing kinetics and thermal-mechanical properties of DGEBA thermosets cured with a hyperbranched poly(ethyleneimine) and an aliphatic triamine. Thermochim Acta 2011;526:9–21. https://doi.org/10.1016/j.tca.2011.08.016.
[59] Galy J, Sabra A, Pascault J. Characterization of epoxy thermosetting systems by differential scanning calorimetry. Polym Eng Sci 1986;26:1514–23. https://doi.org/10.1002/pen.760262108.
[60] Garcia FG, Soares BG, Pita VJRR, Sánchez R, Rieumont J. Mechanical properties of epoxy networks based on DGEBA and aliphatic amines. J Appl Polym Sci 2007;106:2047–55. https://doi.org/10.1002/app.24895.
[61] Javdanitehran M, Berg DC, Duemichen E, Ziegmann G. An iterative approach for isothermal curing kinetics modelling of an epoxy resin system. Thermochim Acta 2016;623:72–9. https://doi.org/10.1016/j.tca.2015.11.014.